



*The University of Michigan*

**"Where am I?"**

**Sensors and Methods for  
Mobile Robot Positioning**

by

**J. Borenstein, H. R. Everett, and L. Feng**

**Edited and Compiled by J. Borenstein**

Contributing Authors: S. W. Lee and R. H. Byrne

Prepared by

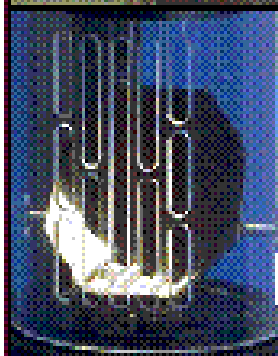
**The University of Michigan**

for the

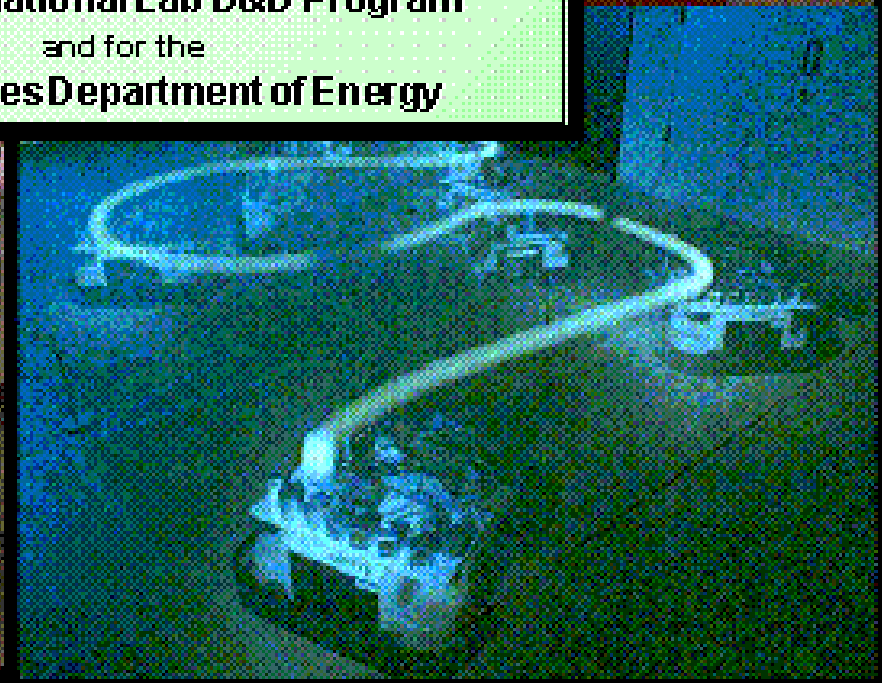
**Oak Ridge National Lab D&D Program**

and for the

**United States Department of Energy**



**TAC  
LightRang**



*The University of Michigan*

**Where am I?  
Sensors and Methods for  
Mobile Robot Positioning**

by

**J. Borenstein<sup>1</sup>, H. R. Everett<sup>2</sup>, and L. Feng<sup>3</sup>**

**Contributing authors: S. W. Lee and R. H. Byrne**

**Edited and compiled by J. Borenstein**

**April 1996**

**Prepared by the University of Michigan  
For the Oak Ridge National Lab (ORNL) D&D Program  
and the  
United States Department of Energy's  
Robotics Technology Development Program  
Within the Environmental Restoration, Decontamination and Dismantlement Project**

---

<sup>1</sup> Dr. Johann Borenstein  
The University of Michigan  
Department of Mechanical  
Engineering and Applied Mechanics  
Mobile Robotics Laboratory  
1101 Beal Avenue  
Ann Arbor, MI 48109  
Ph.: (313) 763-1560  
Fax: (313) 944-1113  
Email: johannb@umich.edu

<sup>2</sup> Commander H. R. Everett  
Naval Command, Control, and  
Ocean Surveillance Center  
RDT&E Division 5303  
271 Catalina Boulevard  
San Diego, CA 92152-5001  
Ph.: (619) 553-3672  
Fax: (619) 553-6188  
Email: Everett@NOSC.MIL

<sup>3</sup> Dr. Liqiang Feng  
The University of Michigan  
Department of Mechanical  
Engineering and Applied Mechanics  
Mobile Robotics Laboratory  
1101 Beal Avenue  
Ann Arbor, MI 48109  
Ph.: (313) 936-9362  
Fax: (313) 763-1260  
Email: Feng@engin.umich.edu

---


*Please direct all inquiries to Johann Borenstein.*

## How to Use this Document

The use of the Acrobat Reader utility is straight-forward; if necessary, help is available from the Help Menu. Here are some tips:

You may wish to enable View => Bookmarks & Page to see a list of bookmarks besides the current page. Clicking on a bookmark will cause the Acrobat Reader to jump directly to the location marked by the bookmark (e.g., the first page in a specific chapter).

You may wish to enable View => Thumbnails & Page to see each page as a small thumbnail-sized image besides the current page. This allows you to quickly locate a page that you remember because of a table or graphics element. Clicking on a thumbnail will cause the Acrobat Reader to jump directly to the page marked by the thumbnail.

Occasionally a term will be marked by a red rectangle, indicating a reference to an external document. Clicking inside the rectangle will automatically load the referenced document and display it. Clicking on the  key will return the Acrobat Reader to the original document.

Occasionally a term will be marked by a blue rectangle. This indicates a link to an external video clip. Clicking inside the blue rectangle will bring up the video player (provided one is installed on your platform).

If you would like to check the video clips, [click here](#) for a list and instructions:

If you would like to contribute your own material for next year's edition of the "Where am I" Report, [click here](#) for instructions.

# *Acknowledgments*

**This research was sponsored by the  
Office of Technology Development, U.S. Department of Energy,  
under contract DE-FG02-86NE37969  
with the University of Michigan**

**Significant portions of the text were adapted from  
"Sensors for Mobile Robots: Theory and Application"  
by H. R. Everett,  
A K Peters, Ltd., Wellesley, MA, Publishers, 1995.**

**Chapter 9 was contributed entirely by  
Sang W. Lee from the Artificial Intelligence Lab  
at the University of Michigan**

**Significant portions of Chapter 3 were adapted from  
"Global Positioning System Receiver Evaluation Results."  
by Raymond H. Byrne, originally published as  
Sandia Report SAND93-0827, Sandia National Laboratories, 1993.**

**The authors wish to thank the Department of Energy (DOE), and especially  
Dr. Linton W. Yarbrough, DOE Program Manager, Dr. William R. Hamel, D&D  
Technical Coordinator, and Dr. Clyde Ward, Landfill Operations Technical  
Coordinator for their technical and financial support of the  
research, which forms the basis of this work.**

**The authors further wish to thank Professors David K. Wehe and Yoram Koren  
at the University of Michigan for their support, and Mr. Harry Alter (DOE)  
who has befriended many of the graduate students and sired several of our robots.**

**Thanks are also due to Todd Ashley Everett for making most of the line-art drawings.**

# Table of Contents

<b>Introduction</b> .....	10
---------------------------	----

## **PART I SENSORS FOR MOBILE ROBOT POSITIONING**

<b>Chapter 1 Sensors for Dead Reckoning</b> .....	13
1.1 Optical Encoders .....	13
1.1.1 Incremental Optical Encoders .....	14
1.1.2 Absolute Optical Encoders .....	16
1.2 Doppler Sensors .....	17
1.2.1 Micro-Trak <i>Trak-Star</i> Ultrasonic Speed Sensor .....	18
1.2.2 Other Doppler-Effect Systems .....	19
1.3 Typical Mobility Configurations .....	19
1.3.1 Differential Drive .....	19
1.3.2 Tricycle Drive .....	21
1.3.3 Ackerman Steering .....	21
1.3.4 Synchro Drive .....	23
1.3.5 Omnidirectional Drive .....	25
1.3.6 Multi-Degree-of-Freedom Vehicles .....	26
1.3.7 MDOF Vehicle with Compliant Linkage .....	27
1.3.8 Tracked Vehicles .....	28
<b>Chapter 2 Heading Sensors</b> .....	30
2.1 Mechanical Gyroscopes .....	30
2.1.1 Space-Stable Gyroscopes .....	31
2.1.2 Gyrocompasses .....	32
2.1.3 Commercially Available Mechanical Gyroscopes .....	32
2.1.3.1 Futaba Model Helicopter Gyro .....	33
2.1.3.2 Gyration, Inc. .....	33
2.2 Piezoelectric Gyroscopes .....	33
2.3 Optical Gyroscopes .....	34
2.3.1 Active Ring Laser Gyros .....	36
2.3.2 Passive Ring Resonator Gyros .....	38
2.3.3 Open-Loop Interferometric Fiber Optic Gyros .....	39
2.3.4 Closed-Loop Interferometric Fiber Optic Gyros .....	42
2.3.5 Resonant Fiber Optic Gyros .....	42
2.3.6 Commercially Available Optical Gyroscopes .....	43
2.3.6.1 The Andrew "Autogyro" .....	43
2.3.6.2 Hitachi Cable Ltd. OFG-3 .....	44
2.4 Geomagnetic Sensors .....	45
2.4.1 Mechanical Magnetic Compasses .....	46
2.4.2 Fluxgate Compasses .....	47
2.4.2.1 Zemco Fluxgate Compasses .....	52

2.4.2.2 Watson Gyrocompass .....	55
2.4.2.3 KVH Fluxgate Compasses .....	56
2.4.3 Hall-Effect Compasses .....	57
2.4.4 Magnetoresistive Compasses .....	59
2.4.4.1 Philips AMR Compass .....	59
2.4.5 Magnetoelastic Compasses .....	60
<b>Chapter 3 Ground-Based RF-Beacons and GPS .....</b>	<b>65</b>
3.1 Ground-Based RF Systems .....	65
3.1.1 Loran .....	65
3.1.2 Kaman Sciences <i>Radio Frequency Navigation Grid</i> .....	66
3.1.3 Precision Location Tracking and Telemetry System .....	67
3.1.4 Motorola <i>Mini-Ranger Falcon</i> .....	68
3.1.5 Harris <i>Infogeometric</i> System .....	69
3.2 Overview of Global Positioning Systems (GPSs) .....	70
3.3 Evaluation of Five GPS Receivers by Byrne [1993] .....	78
3.3.1 Project Goals .....	78
3.3.2 Test Methodology .....	78
3.3.2.1 Parameters tested .....	79
3.3.2.2 Test hardware .....	81
3.3.2.3 Data post processing .....	82
3.3.3 Test Results .....	83
3.3.3.1 Static test results .....	84
3.3.3.2 Dynamic test results .....	88
3.3.3.3 Summary of test results .....	91
3.3.4 Recommendations .....	91
3.3.4.1 Summary of problems encountered with the tested GPS receivers .....	92
3.3.4.2 Summary of critical integration issues .....	92
<b>Chapter 4 Sensors for Map-Based Positioning .....</b>	<b>95</b>
4.1 Time-of-Flight Range Sensors .....	95
4.1.1 Ultrasonic TOF Systems .....	97
4.1.1.1 Massa Products Ultrasonic Ranging Module Subsystems .....	97
4.1.1.2 Polaroid Ultrasonic Ranging Modules .....	99
4.1.2 Laser-Based TOF Systems .....	101
4.1.2.1 Schwartz Electro-Optics Laser Rangefinders .....	101
4.1.2.2 RIEGL Laser Measurement Systems .....	107
4.1.2.3 RVSI Long Optical Ranging and Detection System .....	109
4.2 Phase-Shift Measurement .....	112
4.2.1 Odetics Scanning Laser Imaging System .....	115
4.2.2 ESP <i>Optical Ranging System</i> .....	116
4.2.3 Acuity Research <i>AccuRange 3000</i> .....	117
4.2.4 TRC Light Direction and Ranging System .....	119
4.2.5 Swiss Federal Institute of Technology's "3-D Imaging Scanner" .....	120
4.2.6 Improving Lidar Performance .....	121
4.3 Frequency Modulation .....	123

4.3.1 Eaton VORAD Vehicle Detection and Driver Alert System .....	125
4.3.2 Safety First Systems Vehicular Obstacle Detection and Warning System .....	127

## **PART II SYSTEMS AND METHODS FOR MOBILE ROBOT POSITIONING**

<b>Chapter 5 Odometry and Other Dead-Reckoning Methods .....</b>	<b>130</b>
5.1 Systematic and Non-Systematic Odometry Errors .....	130
5.2 Measurement of Odometry Errors .....	132
5.2.1 Measurement of Systematic Odometry Errors .....	132
5.2.1.1 The Unidirectional Square-Path Test .....	132
5.2.1.2 The Bidirectional Square-Path Experiment .....	134
5.2.2 Measurement of Non-Systematic Errors .....	136
5.3 Reduction of Odometry Errors .....	137
5.3.1 Reduction of Systematic Odometry Errors .....	138
5.3.1.1 Auxiliary Wheels and Basic Encoder Trailer .....	138
5.3.1.2 The Basic Encoder Trailer .....	139
5.3.1.3 Systematic Calibration .....	139
5.3.2 Reducing Non-Systematic Odometry Errors .....	143
5.3.2.1 Mutual Referencing .....	143
5.3.2.2 Internal Position Error Correction .....	143
5.4 Inertial Navigation .....	145
5.4.1 Accelerometers .....	146
5.4.2 Gyros .....	146
5.4.2.1 Barshan and Durrant-Whyte [1993; 1994; 1995] .....	147
5.4.2.2 Komoriya and Oyama [1994] .....	148
5.5 Summary .....	149
<b>Chapter 6 Active Beacon Navigation Systems .....</b>	<b>151</b>
6.1 Discussion on Triangulation Methods .....	152
6.1.1 Three-Point Triangulation .....	152
6.1.2 Triangulation with More Than Three Landmarks .....	153
6.2 Ultrasonic Transponder Trilateration .....	154
6.2.1 IS Robotics 2-D Location System .....	155
6.2.2 Tulane University 3-D Location System .....	155
6.3 Optical Positioning Systems .....	157
6.3.1 Cybermotion Docking Beacon .....	158
6.3.2 <i>Hilare</i> .....	159
6.3.3 NAMCO LASERNET .....	160
6.3.3.1 U.S. Bureau of Mines' application of the LaserNet sensor .....	161
6.3.4 Denning Branch International Robotics <i>LaserNav Position Sensor</i> .....	163
6.3.5 TRC Beacon Navigation System .....	163
6.3.6 Siman Sensors and Intelligent Machines Ltd., <i>ROBOSENSE</i> .....	164
6.3.7 Imperial College Beacon Navigation System .....	165
6.3.8 MTI Research CONAC™ .....	166
6.3.9 Spatial Positioning Systems, inc.: <i>Odyssey</i> .....	170

6.4 Summary .....	172
<b>Chapter 7 Landmark Navigation .....</b>	<b>173</b>
7.1 Natural Landmarks .....	174
7.2 Artificial Landmarks .....	175
7.2.1 Global Vision .....	176
7.3 Artificial Landmark Navigation Systems .....	176
7.3.1 MDARS Lateral-Post Sensor .....	177
7.3.2 Caterpillar <i>Self Guided Vehicle</i> .....	178
7.3.3 Komatsu Ltd, <i>Z-shaped landmark</i> .....	179
7.4 Line Navigation .....	180
7.4.1 Thermal Navigational Marker .....	181
7.4.2 Volatile Chemicals Navigational Marker .....	181
7.5 Summary .....	183
<b>Chapter 8 Map-based Positioning .....</b>	<b>184</b>
8.1 Map Building .....	185
8.1.1 Map-Building and Sensor Fusion .....	186
8.1.2 Phenomenological vs. Geometric Representation, Engelson & McDermott [1992] .....	186
8.2 Map Matching .....	187
8.2.1 Schiele and Crowley [1994] .....	188
8.2.2 Hinkel and Knieriemen [1988] — <i>The Angle Histogram</i> .....	189
8.2.3 Weiß, Wetzler, and Puttkamer — <i>More on the Angle Histogram</i> .....	191
8.2.4 Siemens' <i>Roamer</i> .....	193
8.2.5 Bauer and Rencken: Path Planning for Feature-based Navigation .....	194
8.3 Geometric and Topological Maps .....	196
8.3.1 Geometric Maps for Navigation .....	197
8.3.1.1 Cox [1991] .....	198
8.3.1.2 Crowley [1989] .....	199
8.3.1.3 Adams and von Flüe .....	202
8.3.2 Topological Maps for Navigation .....	203
8.3.2.1 Taylor [1991] .....	203
8.3.2.2 Courtney and Jain [1994] .....	203
8.3.2.3 Kortenkamp and Weymouth [1993] .....	204
8.4 Summary .....	206



Chapter 9 Vision-Based Positioning .....	207
9.1 Camera Model and Localization .....	207
9.2 Landmark-Based Positioning .....	209
9.2.1 Two-Dimensional Positioning Using a Single Camera .....	209
9.2.2 Two-Dimensional Positioning Using Stereo Cameras .....	211
9.3 Camera-Calibration Approaches .....	211
9.4 Model-Based Approaches .....	213
9.4.1 Three-Dimensional Geometric Model-Based Positioning .....	214
9.4.2 Digital Elevation Map-Based Localization .....	215
9.5 Feature-Based Visual Map Building .....	215
9.6 Summary and Discussion .....	216
Appendix A A Word on Kalman Filters .....	218
Appendix B Unit Conversions and Abbreviations .....	219
Appendix C Systems-at-a-Glance Tables .....	221
References .....	236
Subject Index .....	262
Author Index .....	274
Company Index .....	278
Bookmark Index .....	279
Video Index .....	280
Full-length Papers Index .....	281

# INTRODUCTION

Leonard and Durrant-Whyte [1991] summarized the general problem of mobile robot navigation by three questions: “Where am I?,” “Where am I going?,” and “How should I get there?.” This report surveys the state-of-the-art in sensors, systems, methods, and technologies that aim at answering the first question, that is: robot positioning in its environment.

Perhaps the most important result from surveying the vast body of literature on mobile robot positioning is that to date there is no truly elegant solution for the problem. The many partial solutions can roughly be categorized into two groups: *relative* and *absolute* position measurements. Because of the lack of a single, generally good method, developers of *automated guided vehicles* (AGVs) and mobile robots usually combine two methods, one from each category. The two categories can be further divided into the following subgroups.

## Relative Position Measurements

- a. **Odometry** This method uses encoders to measure wheel rotation and/or steering orientation. Odometry has the advantage that it is totally self-contained, and it is always capable of providing the vehicle with an estimate of its position. The disadvantage of odometry is that the position error grows without bound unless an independent reference is used periodically to reduce the error [Cox, 1991].
- b. **Inertial Navigation** This method uses gyroscopes and sometimes accelerometers to measure rate of rotation and acceleration. Measurements are integrated once (or twice) to yield position. Inertial navigation systems also have the advantage that they are self-contained. On the downside, inertial sensor data drifts with time because of the need to integrate rate data to yield position; any small constant error increases without bound after integration. Inertial sensors are thus unsuitable for accurate positioning over an extended period of time. Another problem with inertial navigation is the high equipment cost. For example, highly accurate gyros, used in airplanes, are prohibitively expensive. Very recently fiber-optic gyros (also called laser gyros), which are said to be very accurate, have fallen dramatically in price and have become a very attractive solution for mobile robot navigation.

## Absolute Position Measurements

- c. **Active Beacons** This method computes the absolute position of the robot from measuring the direction of incidence of three or more actively transmitted beacons. The transmitters, usually using light or radio frequencies, must be located at known sites in the environment.
- d. **Artificial Landmark Recognition** In this method distinctive artificial landmarks are placed at known locations in the environment. The advantage of artificial landmarks is that they can be designed for optimal detectability even under adverse environmental conditions. As with active beacons, three or more landmarks must be “in view” to allow position estimation. Landmark positioning has the advantage that the position errors are bounded, but detection of external

landmarks and real-time position fixing may not always be possible. Unlike the usually point-shaped beacons, artificial landmarks may be defined as a set of features, e.g., a shape or an area. Additional information, for example distance, can be derived from measuring the geometric properties of the landmark, but this approach is computationally intensive and not very accurate.

- e. **Natural Landmark Recognition** Here the landmarks are distinctive features in the environment. There is no need for preparation of the environment, but the environment must be known in advance. The reliability of this method is not as high as with artificial landmarks.
- f. **Model Matching** In this method information acquired from the robot's onboard sensors is compared to a map or world model of the environment. If features from the sensor-based map and the world model map match, then the vehicle's absolute location can be estimated. Map-based positioning often includes improving global maps based on the new sensory observations in a dynamic environment and integrating local maps into the global map to cover previously unexplored areas. The maps used in navigation include two major types: geometric maps and topological maps. Geometric maps represent the world in a global coordinate system, while topological maps represent the world as a network of nodes and arcs.

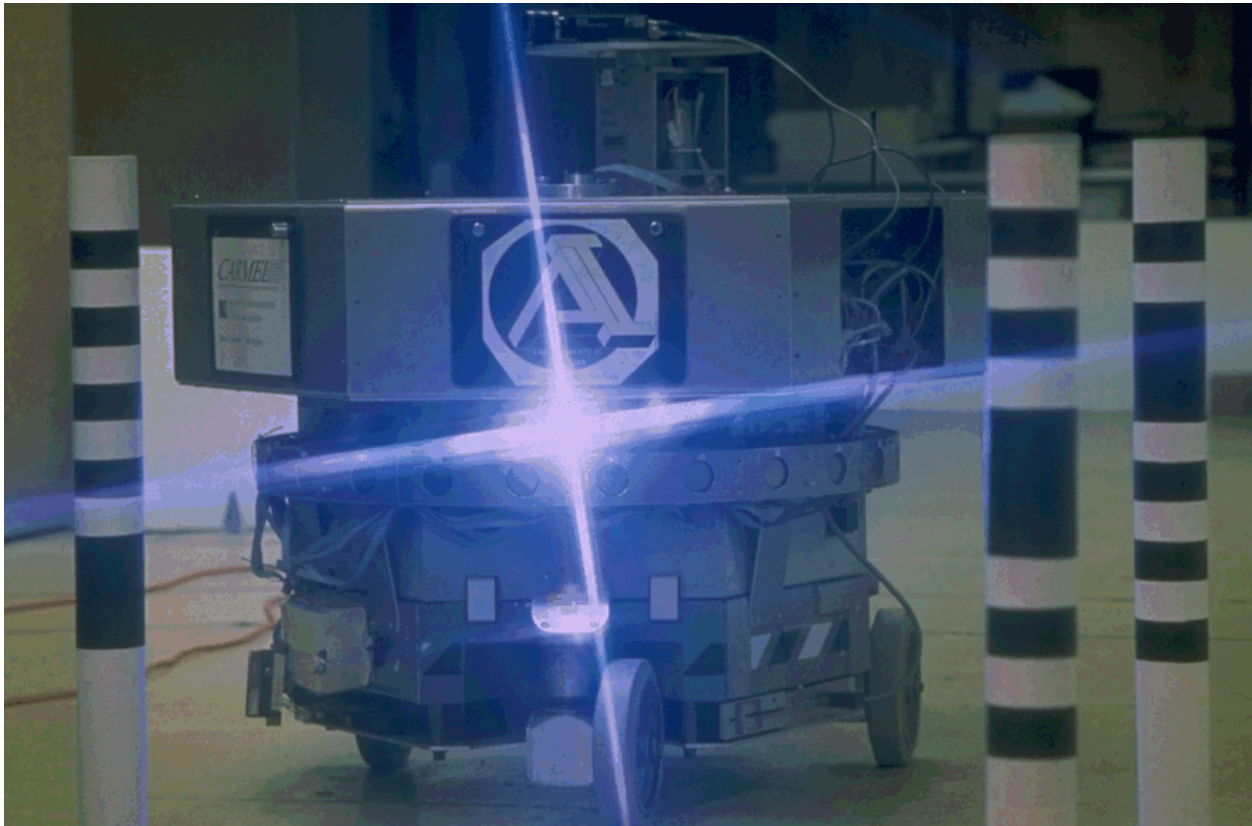
This book presents and discusses the state-of-the-art in each of the above six categories. The material is organized in two parts: Part I deals with the sensors used in mobile robot positioning, and Part II discusses the methods and techniques that make use of these sensors.

Mobile robot navigation is a very diverse area, and a useful comparison of different approaches is difficult because of the lack of commonly accepted test standards and procedures. The research platforms used differ greatly and so do the key assumptions used in different approaches. Further difficulty arises from the fact that different systems are at different stages in their development. For example, one system may be commercially available, while another system, perhaps with better performance, has been tested only under a limited set of laboratory conditions. For these reasons we generally refrain from comparing or even judging the performance of different systems or techniques. Furthermore, we have not tested most of the systems and techniques, so the results and specifications given in this book are merely quoted from the respective research papers or product spec-sheets.

Because of the above challenges we have defined the purpose of this book to be a survey of the expanding field of mobile robot positioning. It took well over 1.5 man-years to gather and compile the material for this book; we hope this work will help the reader to gain greater understanding in much less time.

# Part I

## Sensors for Mobile Robot Positioning



CARMEL, the University of Michigan's first mobile robot, has been in service since 1987. Since then, CARMEL has served as a reliable testbed for countless sensor systems. In the extra "shelf" underneath the robot is an 8086 XT compatible single-board computer that runs U of M's ultrasonic sensor firing algorithm. Since this code was written in 1987, the computer has been booting up and running from *floppy disk*. The program was written in FORTH and was never altered; should anything ever go wrong with the floppy, it will take a computer *historian* to recover the code...

# CHAPTER 1

## SENSORS FOR DEAD RECKONING

*Dead reckoning* (derived from “deduced reckoning” of sailing days) is a simple mathematical procedure for determining the present location of a vessel by advancing some previous position through known course and velocity information over a given length of time [Dunlap and Shufeldt, 1972]. The vast majority of land-based mobile robotic systems in use today rely on dead reckoning to form the very backbone of their navigation strategy, and like their nautical counterparts, periodically null out accumulated errors with recurring “fixes” from assorted navigation aids.

The most simplistic implementation of dead reckoning is sometimes termed *odometry*; the term implies vehicle displacement along the path of travel is directly derived from some onboard “odometer.” A common means of odometry instrumentation involves optical encoders directly coupled to the motor armatures or wheel axles.

Since most mobile robots rely on some variation of wheeled locomotion, a basic understanding of sensors that accurately quantify angular position and velocity is an important prerequisite to further discussions of odometry. There are a number of different types of rotational displacement and velocity sensors in use today:

- Brush encoders.
- Potentiometers.
- Synchros.
- Resolvers.
- Optical encoders.
- Magnetic encoders.
- Inductive encoders.
- Capacitive encoders.

A multitude of issues must be considered in choosing the appropriate device for a particular application. Avolio [1993] points out that over 17 million variations on rotary encoders are offered by one company alone. For mobile robot applications incremental and absolute optical encoders are the most popular type. We will discuss those in the following sections.

### 1.1 Optical Encoders

The first optical encoders were developed in the mid-1940s by the Baldwin Piano Company for use as “tone wheels” that allowed electric organs to mimic other musical instruments [Agent, 1991]. Today’s corresponding devices basically embody a miniaturized version of the *break-beam proximity sensor*. A focused beam of light aimed at a matched photodetector is periodically interrupted by a coded opaque/transparent pattern on a rotating intermediate disk attached to the shaft of interest. The rotating disk may take the form of chrome on glass, etched metal, or *photoplast* such as Mylar [Henkel, 1987]. Relative to the more complex alternating-current resolvers, the straightforward encoding scheme and inherently digital output of the optical encoder results in a low-cost reliable package with good noise immunity.

There are two basic types of optical encoders: *incremental* and *absolute*. The incremental version measures rotational velocity and can infer relative position, while absolute models directly measure angular position and infer velocity. If non volatile position information is not a consideration, *incremental encoders* generally are easier to interface and provide equivalent resolution at a much lower cost than *absolute* optical encoders.

### 1.1.1 Incremental Optical Encoders

The simplest type of incremental encoder is a single-channel *tachometer encoder*, basically an instrumented mechanical light chopper that produces a certain number of sine- or square-wave pulses for each shaft revolution. Adding pulses increases the resolution (and subsequently the cost) of the unit. These relatively inexpensive devices are well suited as velocity feedback sensors in medium- to high-speed control systems, but run into noise and stability problems at extremely slow velocities due to quantization errors [Nickson, 1985]. The tradeoff here is resolution versus update rate: improved transient response requires a faster update rate, which for a given line count reduces the number of possible encoder pulses per sampling interval. A very simple, do-it-yourself encoder is described in [Jones and Flynn, 1993]. More sophisticated single-channel encoders are typically limited to 2540 lines for a 5-centimeter (2 in) diameter incremental encoder disk [Henkel, 1987].

In addition to low-speed instabilities, single-channel tachometer encoders are also incapable of detecting the direction of rotation and thus cannot be used as position sensors. *Phase-quadrature incremental encoders* overcome these problems by adding a second channel, displaced from the first, so the resulting pulse trains are 90 degrees out of phase as shown in Figure 1.1. This technique allows the decoding electronics to determine which channel is leading the other and hence ascertain the direction of rotation, with the added benefit of increased resolution. Holle [1990] provides an in-depth discussion of output options (single-ended TTL or differential drivers) and various design issues (i.e., resolution, bandwidth, phasing, filtering) for consideration when interfacing phase-quadrature incremental encoders to digital control systems.

The incremental nature of the phase-quadrature output signals dictates that any resolution of angular position can only be relative to some specific reference, as opposed to absolute. Establishing such a reference can be accomplished in a number of ways. For applications involving continuous 360-degree rotation, most encoders incorporate as a third channel a special *index output* that goes high once for each complete revolution of the shaft (see Figure 1.1 above). Intermediate shaft

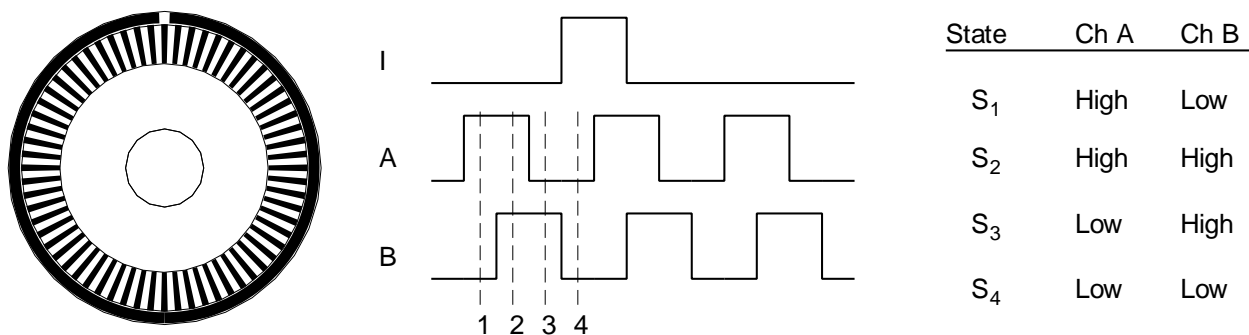


**Figure 1.1:** The observed phase relationship between Channel A and B pulse trains can be used to determine the direction of rotation with a phase-quadrature encoder, while unique output states  $S_1 - S_4$  allow for up to a four-fold increase in resolution. The single slot in the outer track generates one index pulse per disk rotation [Everett, 1995].

positions are then specified by the number of encoder up counts or down counts from this known index position. One disadvantage of this approach is that all relative position information is lost in the event of a power interruption.

In the case of limited rotation, such as the back-and-forth motion of a pan or tilt axis, electrical limit switches and/or mechanical stops can be used to establish a home reference position. To improve repeatability this homing action is sometimes broken into two steps. The axis is rotated at reduced speed in the appropriate direction until the stop mechanism is encountered, whereupon rotation is reversed for a short predefined interval. The shaft is then rotated slowly back into the stop at a specified low velocity from this designated start point, thus eliminating any variations in inertial loading that could influence the final homing position. This two-step approach can usually be observed in the power-on initialization of stepper-motor positioners for dot-matrix printer heads.

Alternatively, the absolute indexing function can be based on some external referencing action that is decoupled from the immediate servo-control loop. A good illustration of this situation involves an incremental encoder used to keep track of platform steering angle. For example, when the *K2A Navmaster* [CYBERMOTION] robot is first powered up, the absolute steering angle is unknown, and must be initialized through a “referencing” action with the docking beacon, a nearby wall, or some other identifiable set of landmarks of known orientation. The up/down count output from the decoder electronics is then used to modify the vehicle heading register in a relative fashion.

A growing number of very inexpensive off-the-shelf components have contributed to making the phase-quadrature incremental encoder the rotational sensor of choice within the robotics research and development community. Several manufacturers now offer small DC gear-motors with incremental encoders already attached to the armature shafts. Within the U.S. automated guided vehicle (AGV) industry, however, resolvers are still generally preferred over optical encoders for their perceived superiority under harsh operating conditions, but the European AGV community seems to clearly favor the encoder [Manolis, 1993].

Interfacing an incremental encoder to a computer is not a trivial task. A simple state-based interface as implied in Figure 1.1 is inaccurate if the encoder changes direction at certain positions, and false pulses can result from the interpretation of the sequence of state changes [Pessen, 1989]. Pessen describes an accurate circuit that correctly interprets directional state changes. This circuit was originally developed and tested by Borenstein [1987].

A more versatile encoder interface is the HCTL 1100 motion controller chip made by Hewlett Packard [HP]. The HCTL chip performs not only accurate quadrature decoding of the incremental wheel encoder output, but it provides many important additional functions, including among others:

- closed-loop position control,
- closed-loop velocity control in P or PI fashion,
- 24-bit position monitoring.

At the University of Michigan's Mobile Robotics Lab, the HCTL 1100 has been tested and used in many different mobile robot control interfaces. The chip has proven to work reliably and accurately, and it is used on commercially available mobile robots, such as the TRC *LabMate* and *HelpMate*. The HCTL 1100 costs only \$40 and it comes highly recommended.

### 1.1.2 Absolute Optical Encoders

Absolute encoders are typically used for slower rotational applications that require positional information when potential loss of reference from power interruption cannot be tolerated. Discrete detector elements in a photovoltaic array are individually aligned in break-beam fashion with concentric encoder tracks as shown in Figure 1.2, creating in effect a non-contact implementation of a commutating brush encoder. The assignment of a dedicated track for each bit of resolution results in larger size disks (relative to incremental designs), with a corresponding decrease in shock and vibration tolerance. A general rule of thumb is that each additional encoder track doubles the resolution but quadruples the cost [Agent, 1991].

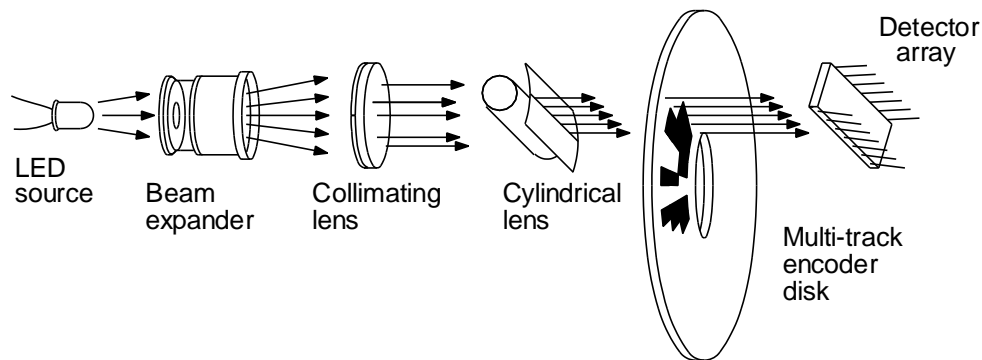


**Figure 1.2:** A line source of light passing through a coded pattern of opaque and transparent segments on the rotating encoder disk results in a parallel output that uniquely specifies the absolute angular position of the shaft. (Adapted from [Agent, 1991].)

Instead of the serial bit streams of incremental designs, absolute optical encoders provide a parallel word output with a unique code pattern for each quantized shaft position. The most common coding schemes are Gray code, natural binary, and binary-coded decimal [Avolio, 1993]. The Gray code (for inventor Frank Gray of Bell Labs) is characterized by the fact that only one bit changes at a time, a decided advantage in eliminating asynchronous ambiguities caused by electronic and mechanical component tolerances (see Figure 1.3a). Binary code, on the other hand, routinely involves multiple bit changes when incrementing or decrementing the count by one. For example, when going from position 255 to position 0 in Figure 1.3b, eight bits toggle from 1s to 0s. Since there is no guarantee all threshold detectors monitoring the detector elements tracking each bit will toggle at the same precise instant, considerable ambiguity can exist during state transition with a coding scheme of this form. Some type of handshake line signaling valid data available would be required if more than one bit were allowed to change between consecutive encoder positions.

Absolute encoders are best suited for slow and/or infrequent rotations such as steering angle encoding, as opposed to measuring high-speed continuous (i.e., drive wheel) rotations as would be required for calculating displacement along the path of travel. Although not quite as robust as resolvers for high-temperature, high-shock applications, absolute encoders can operate at temperatures over 125°C, and medium-resolution (1000 counts per revolution) metal or Mylar disk designs can compete favorably with resolvers in terms of shock resistance [Manolis, 1993]. A potential disadvantage of absolute encoders is their parallel data output, which requires a more complex interface due to the large number of electrical leads. A 13-bit absolute encoder using



complimentary output signals for noise immunity would require a 28-conductor cable (13 signal pairs plus power and ground), versus only six for a resolver or incremental encoder [Avolio, 1993].

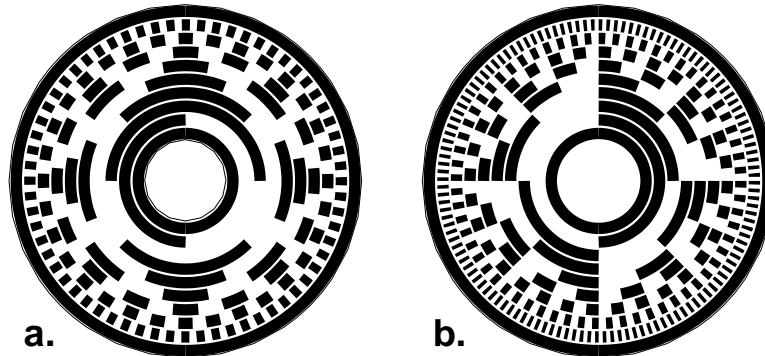


**Figure 1.3:** Rotating an 8-bit absolute Gray code disk.  
 a. Counterclockwise rotation by one position increment will cause only one bit to change.  
 b. The same rotation of a binary-coded disk will cause all bits to change in the particular case (255 to 0) illustrated by the reference line at 12 o'clock.  
 [Everett, 1995].

## 1.2 Doppler Sensors

The rotational displacement sensors discussed above derive navigation parameters directly from wheel rotation, and are thus subject to problems arising from slippage, tread wear, and/or improper tire inflation. In certain applications, Doppler and inertial navigation techniques are sometimes employed to reduce the effects of such error sources.

Doppler navigation systems are routinely employed in maritime and aeronautical applications to yield velocity measurements with respect to the earth itself, thus eliminating dead-reckoning errors introduced by unknown ocean or air currents. The principle of operation is based on the Doppler shift in frequency observed when radiated energy reflects off a surface that is moving with respect to the emitter. Maritime systems employ acoustical energy reflected from the ocean floor, while airborne systems sense microwave RF energy bounced off the surface of the earth. Both configurations typically involve an array of four transducers spaced 90 degrees apart in azimuth and inclined downward at a common angle with respect to the horizontal plane [Dunlap and Shufeldt, 1972].

Due to cost constraints and the reduced likelihood of transverse drift, most robotic implementations employ but a single forward-looking transducer to measure ground speed in the direction of travel. Similar configurations are sometimes used in the agricultural industry, where tire slippage in soft freshly plowed dirt can seriously interfere with the need to release seed or fertilizer at a rate commensurate with vehicle advance. The M113-based Ground Surveillance Vehicle [Harmon, 1986] employed an off-the-shelf unit of this type manufactured by John Deere to compensate for track slippage.

The microwave radar sensor is aimed downward at a prescribed angle (typically  $45^\circ$ ) to sense ground movement as shown in Figure 1.4. Actual ground speed  $V_A$  is derived from the measured velocity  $V_D$  according to the following equation [Schultz, 1993]:

$$V_A = \frac{V_D}{\cos\alpha} = \frac{cF_D}{2F_0 \cos\alpha} \quad (1.1)$$

where

- $V_A$  = actual ground velocity along path
- $V_D$  = measured Doppler velocity
- $\alpha$  = angle of declination
- $c$  = speed of light
- $F_D$  = observed Doppler shift frequency
- $F_0$  = transmitted frequency.

Errors in detecting true ground speed arise due to side-lobe interference, vertical velocity components introduced by vehicle reaction to road surface anomalies, and uncertainties in the actual angle of incidence due to the finite width of the beam. Byrne et al. [1992] point out another interesting scenario for potentially erroneous operation, involving a stationary vehicle parked over a stream of water. The Doppler ground-speed sensor in this case would misinterpret the relative motion between the stopped vehicle and the running water as vehicle travel.

### 1.2.1 Micro-Trak *Trak-Star* Ultrasonic Speed Sensor

One commercially available speed sensor that is based on Doppler speed measurements is the *Trak-Star* Ultrasonic Speed Sensor [MICRO-TRAK]. This device, originally designed for agricultural applications, costs \$420. The manufacturer claims that this is the most accurate Doppler speed sensor available. The technical specifications are listed in Table 1.1.

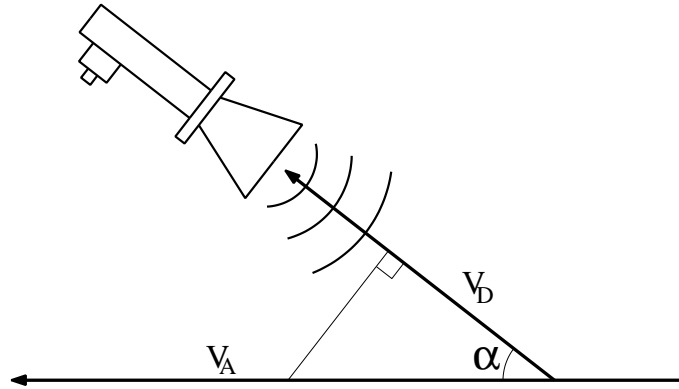


**Figure 1.4:** A Doppler ground-speed sensor inclined at an angle  $\alpha$  as shown measures the velocity component  $V_D$  of true ground speed  $V_A$ . (Adapted from [Schultz, 1993].)

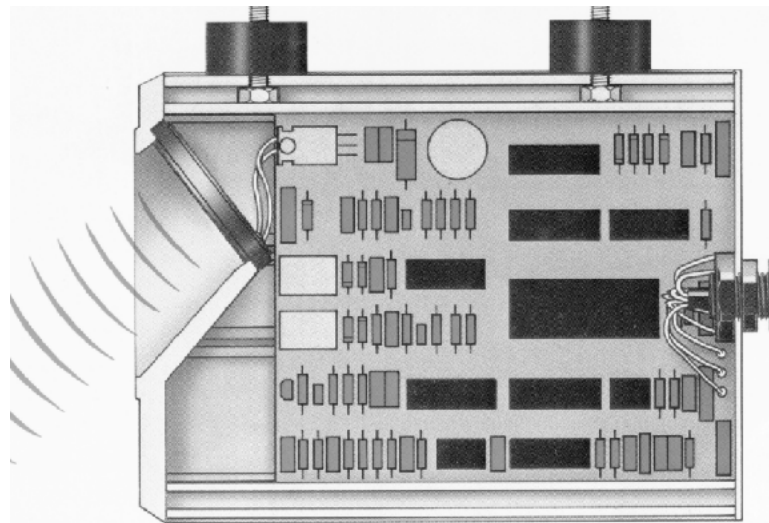


**Figure 1.5:** The *Trak-Star* Ultrasonic Speed Sensor is based on the Doppler effect. This device is primarily targeted at the agricultural market. (Courtesy of Micro-Trak.)

### 1.2.2 Other Doppler-Effect Systems

A non-radar Doppler-effect device is the *Monitor 1000*, a distance and speed monitor for runners. This device was temporarily marketed by the sporting goods manufacturer [NIKE]. The *Monitor 1000* was worn by the runner like a front-mounted fanny pack. The small and lightweight device used ultrasound as the carrier, and was said to have an accuracy of two to five percent, depending on the ground characteristics. The manufacturer of the *Monitor 1000* is Applied Design Laboratories [ADL]. A microwave radar Doppler effect distance sensor has also been developed by ADL. This radar sensor is a prototype and is not commercially available. However, it differs from the *Monitor 1000* only in its use of a radar sensor head as opposed to the ultrasonic sensor head used by the *Monitor 1000*. The prototype radar sensor measures  $15 \times 10 \times 5$  centimeters ( $6 \times 4 \times 2$  in), weighs 250 grams (8.8 oz), and consumes 0.9 W.

**Table 1.1:** Specifications for the *Trak-Star* Ultrasonic Speed Sensor.

Parameter	Value	Units
Speed range	17.7	m/s
	0-40	mph
Speed resolution	1.8	cm/s
	0.7	in/s
Accuracy	$\pm 1.5\% + 0.04$	mph
Transmit frequency	62.5	kHz
Temperature range	-29 to +50	$^{\circ}\text{C}$
	-20 to +120	$^{\circ}\text{F}$
Weight	1.3	kg
	3	lb
Power requirements	12	VDC
	0.03	A

## 1.3 Typical Mobility Configurations

The accuracy of odometry measurements for dead reckoning is to a great extent a direct function of the kinematic design of a vehicle. Because of this close relation between kinematic design and positioning accuracy, one must consider the kinematic design closely before attempting to improve dead-reckoning accuracy. For this reason, we will briefly discuss some of the more popular vehicle designs in the following sections. In Part II of this report, we will discuss some recently developed methods for reducing odometry errors (or the feasibility of doing so) for some of these vehicle designs.

### 1.3.1 Differential Drive

Figure 1.6 shows a typical *differential drive* mobile robot, the *LabMate* platform, manufactured by [TRC]. In this design incremental encoders are mounted onto the two drive motors to count the wheel revolutions. The robot can perform dead reckoning by using simple geometric equations to compute the momentary position of the vehicle relative to a known starting position.

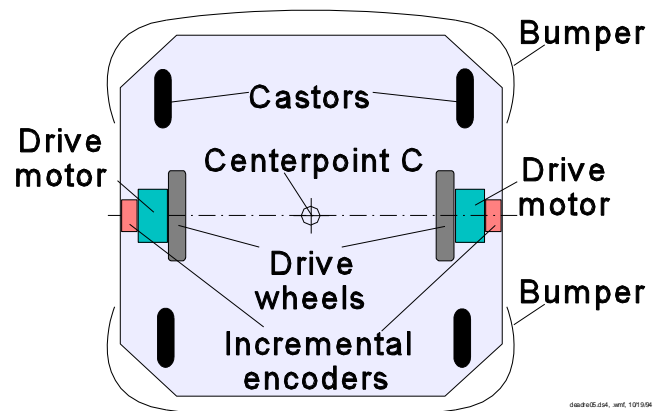


**Figure 1.6:** A typical differential-drive mobile robot (bottom view).

For completeness, we rewrite the well-known equations for odometry below (also, see [Klarer, 1988; Crowley and Reigner, 1992]). Suppose that at sampling interval  $I$  the left and right wheel encoders show a pulse increment of  $N_L$  and  $N_R$ , respectively. Suppose further that

$$c_m = \pi D_n / n C_e \quad (1.2)$$

where

- $c_m$  = conversion factor that translates encoder pulses into linear wheel displacement
- $D_n$  = nominal wheel diameter (in mm)
- $C_e$  = encoder resolution (in pulses per revolution)
- $n$  = gear ratio of the reduction gear between the motor (where the encoder is attached) and the drive wheel.

We can compute the incremental travel distance for the left and right wheel,  $\Delta U_{L,i}$  and  $\Delta U_{R,i}$ , according to

$$\Delta U_{L/R,i} = c_m N_{L/R,i} \quad (1.3)$$

and the incremental linear displacement of the robot's centerpoint  $C$ , denoted  $\Delta U_i$ , according to

$$\Delta U_i = (\Delta U_R + \Delta U_L) / 2. \quad (1.4)$$

Next, we compute the robot's incremental change of orientation

$$\Delta \theta_i = (\Delta U_R - \Delta U_L) / b \quad (1.5)$$

where  $b$  is the wheelbase of the vehicle, ideally measured as the distance between the two contact points between the wheels and the floor.

The robot's new relative orientation  $\theta_i$  can be computed from

$$\theta_i = \theta_{i-1} + \Delta \theta_i \quad (1.6)$$

and the relative position of the centerpoint is

$$x_i = x_{i-1} + \Delta U_i \cos \theta_i \quad (1.7a)$$

$$y_i = y_{i-1} + \Delta U_i \sin \theta_i \quad (1.7b)$$

where

$x_i, y_i$  = relative position of the robot's centerpoint  $c$  at instant  $i$ .

### 1.3.2 Tricycle Drive

Tricycle-drive configurations (see Figure 1.7) employing a single driven front wheel and two passive rear wheels (or vice versa) are fairly common in AGV applications because of their inherent simplicity. For odometry instrumentation in the form of a steering-angle encoder, the dead-reckoning solution is equivalent to that of an Ackerman-steered vehicle, where the steerable wheel replaces the imaginary center wheel discussed in Section 1.3.3. Alternatively, if rear-axle differential odometry is used to determine heading, the solution is identical to the differential-drive configuration discussed in Section 1.3.1.

One problem associated with the tricycle-drive configuration is that the vehicle's center of gravity tends to move away from the front wheel when traversing up an incline, causing a loss of traction. As in the case of Ackerman-steered designs, some surface damage and induced heading errors are possible when actuating the steering while the platform is not moving.

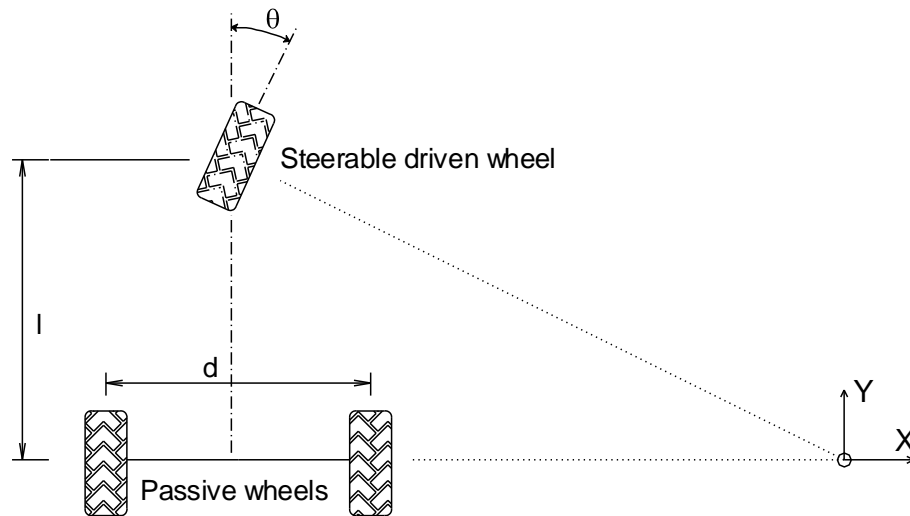


**Figure 1.7:** Tricycle-drive configurations employing a steerable driven wheel and two passive trailing wheels can derive heading information directly from a steering angle encoder or indirectly from differential odometry [Everett, 1995].

### 1.3.3 Ackerman Steering

Used almost exclusively in the automotive industry, Ackerman steering is designed to ensure that the inside front wheel is rotated to a slightly sharper angle than the outside wheel when turning, thereby eliminating geometrically induced tire slippage. As seen in Figure 1.8, the extended axes for the two front wheels intersect in a common point that lies on the extended axis of the rear axle. The locus of points traced along the ground by the center of each tire is thus a set of concentric arcs about this centerpoint of rotation  $P_1$ , and (ignoring for the moment any centrifugal accelerations) all instantaneous velocity vectors will subsequently be tangential to these arcs. Such a steering geometry is said to satisfy the Ackerman equation [Byrne et al., 1992]:

$$\cot\theta_i - \cot\theta_o = \frac{d}{l} \quad (1.8)$$

where

$\theta_i$  = relative steering angle of the inner wheel

$\theta_o$  = relative steering angle of the outer wheel

$l$  = longitudinal wheel separation

$d$  = lateral wheel separation.

For the sake of convenience, the vehicle steering angle  $\theta_{SA}$  can be thought of as the angle (relative to vehicle heading) associated with an imaginary center wheel located at a reference point  $P_2$  as shown in the figure above.  $\theta_{SA}$  can be expressed in terms of either the inside or outside steering angles ( $\theta_i$  or  $\theta_o$ ) as follows [Byrne et al., 1992]:

$$\cot\theta_{SA} = \frac{d}{2l} + \cot\theta_i \quad (1.9)$$

or, alternatively,

$$\cot\theta_{SA} = \cot\theta_o - \frac{d}{2l} \quad (1.10)$$

Ackerman steering provides a fairly accurate odometry solution while supporting the traction and ground clearance needs of all-terrain operation. Ackerman steering is thus the method of choice for outdoor autonomous vehicles. Associated drive implementations typically employ a gasoline or diesel engine coupled to a manual or automatic transmission, with power applied to four wheels through

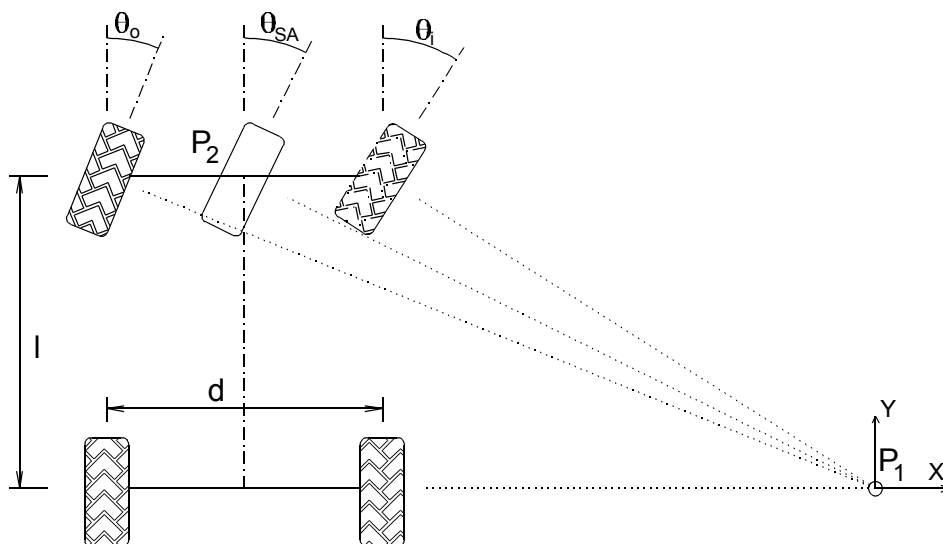


Figure 1.8: In an Ackerman-steered vehicle, the extended axes for all wheels intersect in a common point. (Adapted from [Byrne et al., 1992].)

a transfer case, a differential, and a series of universal joints. A representative example is seen in the HMMWV-based prototype of the USMC Tele-Operated Vehicle (TOV) Program [Aviles et al., 1990]. From a military perspective, the use of existing-inventory equipment of this type simplifies some of the logistics problems associated with vehicle maintenance. In addition, reliability of the drive components is high due to the inherited stability of a proven power train. (Significant interface problems can be encountered, however, in retrofitting off-the-shelf vehicles intended for human drivers to accommodate remote or computer control.)

### 1.3.4 Synchro Drive

An innovative configuration known as synchro drive features three or more wheels (Figure 1.9) mechanically coupled in such a way that all rotate in the same direction at the same speed, and similarly pivot in unison about their respective steering axes when executing a turn. This drive and steering “synchronization” results in improved odometry accuracy through reduced slippage, since all wheels generate equal and parallel force vectors at all times.

The required mechanical synchronization can be accomplished in a number of ways, the most common being a chain, belt, or gear drive. Carnegie Mellon University has implemented an electronically synchronized version on one of their Rover series robots, with dedicated drive motors for each of the three wheels. Chain- and belt-drive configurations experience some degradation in steering accuracy and alignment due to uneven distribution of slack, which varies as a function of loading and direction of rotation. In addition, whenever chains (or timing belts) are tightened to reduce such slack, the individual wheels must be realigned. These problems are eliminated with a completely enclosed gear-drive approach. An enclosed gear train also significantly reduces noise as well as particulate generation, the latter being very important in clean-room applications.

An example of a three-wheeled belt-drive implementation is seen in the Denning Sentry formerly manufactured by Denning Mobile Robots, Woburn, MA [Kadonoff, 1986] and now by Denning Branch Robotics International [DBIR]. Referring to Figure 1.9, drive torque is transferred down through the three steering columns to polyurethane-filled rubber tires. The drive-motor output shaft is mechanically coupled to each of the steering-column power shafts by a heavy-duty timing belt to ensure synchronous operation. A second timing belt transfers the rotational output of the steering motor to the three steering columns, allowing them to synchronously pivot throughout a full 360-

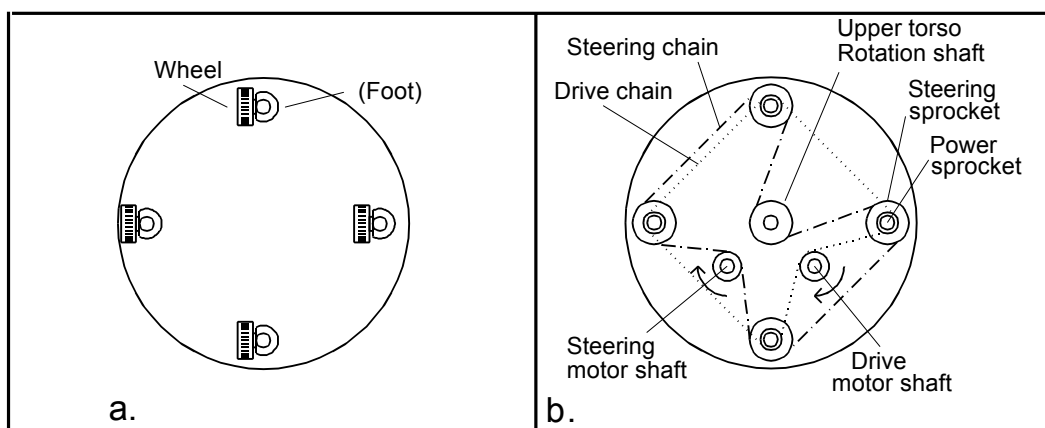


Figure 1.9: A four-wheel synchro-drive configuration: a. Bottom view. b. Top view.  
(Adapted from Holland [1983].)

degree range [Everett, 1985]. The Sentry's upper head assembly is mechanically coupled to the steering mechanism in a manner similar to that illustrated in Figure 1.9, and thus always points in the direction of forward travel. The three-point configuration ensures good stability and traction, while the actively driven large-diameter wheels provide more than adequate obstacle climbing capability for indoor scenarios. The disadvantages of this particular implementation include odometry errors introduced by compliance in the drive belts as well as by reactionary frictional forces exerted by the floor surface when turning in place.

To overcome these problems, the Cybermotion K2A Navmaster robot employs an enclosed gear-drive configuration with the wheels offset from the steering axis as shown in Figure 1.10 and Figure 1.11. When a foot pivots during a turn, the attached wheel rotates in the appropriate direction to minimize floor and tire wear, power consumption, and slippage. Note that for correct compensation, the miter gear on the wheel axis must be on the opposite side of the power shaft gear from the wheel as illustrated. The governing equation for minimal slippage is [Holland, 1983]

$$\frac{A}{B} = \frac{r'}{r} \quad (1.11)$$

where

A = number of teeth on the power shaft gear

B = number of teeth on the wheel axle gear

$r'$  = wheel offset from steering pivot axis

$r$  = wheel radius.

One drawback of this approach is seen in the decreased lateral stability that results when one wheel is turned in under the vehicle. Cybermotion's improved K3A design solves this problem (with an even smaller wheelbase) by incorporating a dual-wheel arrangement on each foot [Fisher et al., 1994]. The two wheels turn in opposite directions in differential fashion as the foot pivots during a turn, but good stability is maintained in the foregoing example by the outward swing of the additional wheel.

The odometry calculations for the synchro drive are almost trivial; vehicle heading is simply derived from the steering-angle encoder, while displacement in the direction of travel is given as follows:

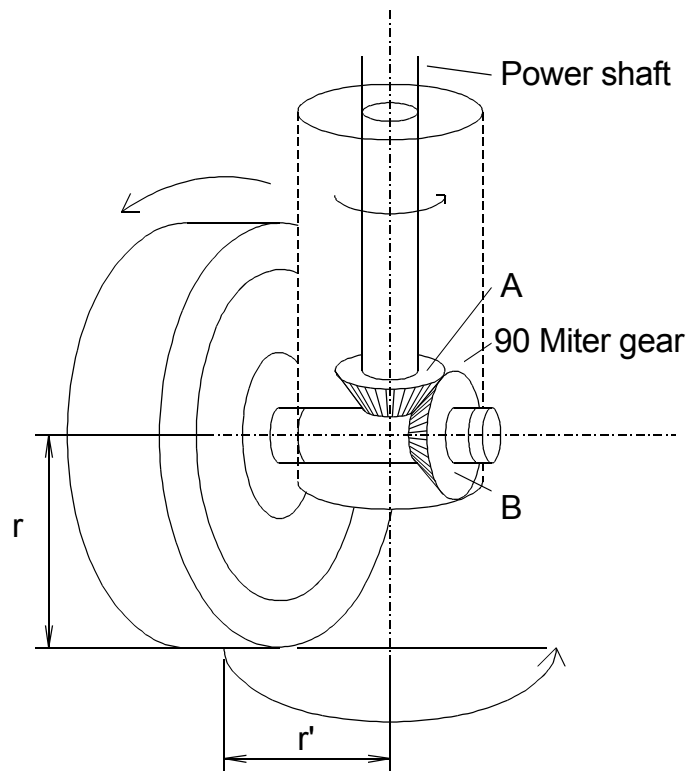
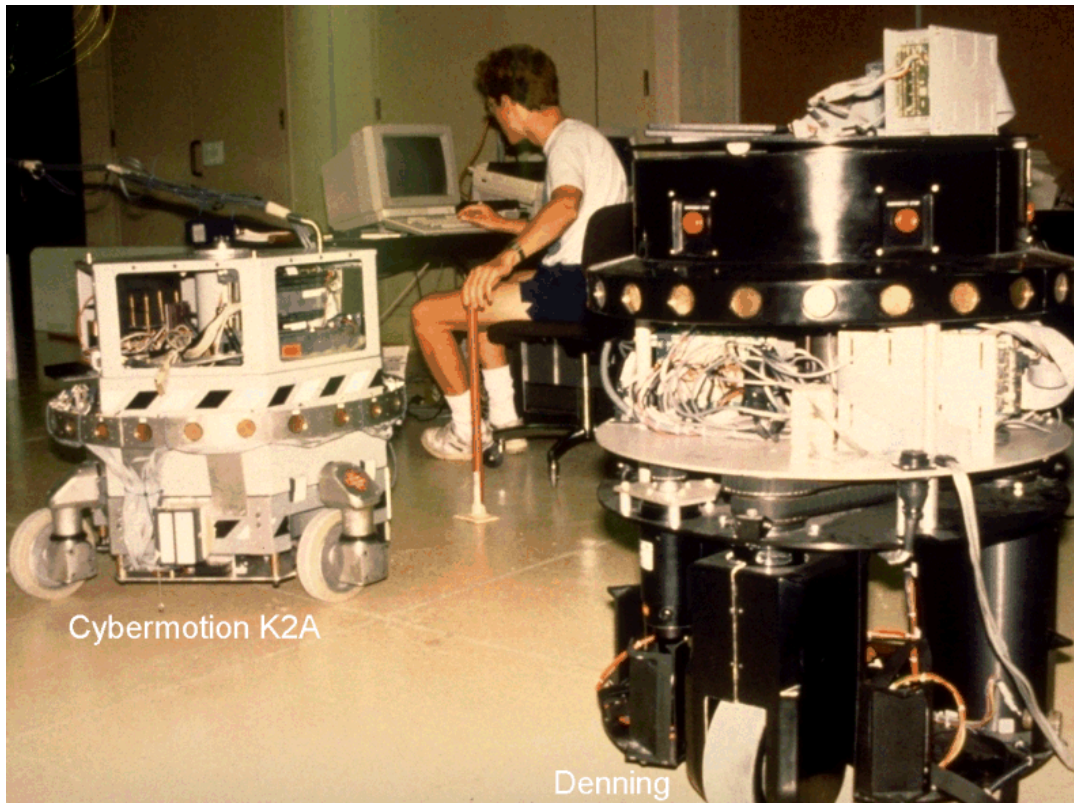


Figure 1.10: Slip compensation during a turn is accomplished through use of an offset foot assembly on the three-wheeled K2A Navmaster robot. (Adapted from [Holland, 1983].)





**Figure 1.11:** The Denning *Sentry* (foreground) incorporates a three-point *synchro-drive* configuration with each wheel located directly below the pivot axis of the associated steering column. In contrast, the Cybermotion K2A (background) has wheels that swivel around the steering column. Both robots were extensively tested at the University of Michigan's Mobile Robotics Lab. (Courtesy of The University of Michigan.)

$$D = \frac{2\pi N}{C_e} R_e \quad (1.12)$$

where

$D$  = vehicle displacement along path

$N$  = measured counts of drive motor shaft encoder

$C_e$  = encoder counts per complete wheel revolution

$R_e$  = effective wheel radius.

### 1.3.5 Omnidirectional Drive

The odometry solution for most multi-degree-of-freedom (MDOF) configurations is done in similar fashion to that for differential drive, with position and velocity data derived from the motor (or wheel) shaft encoders. For the three-wheel example illustrated in Figure 1.12, the equations of motion relating individual motor speeds to velocity components  $V_x$  and  $V_y$  in the reference frame of the vehicle are given by [Holland, 1983]:

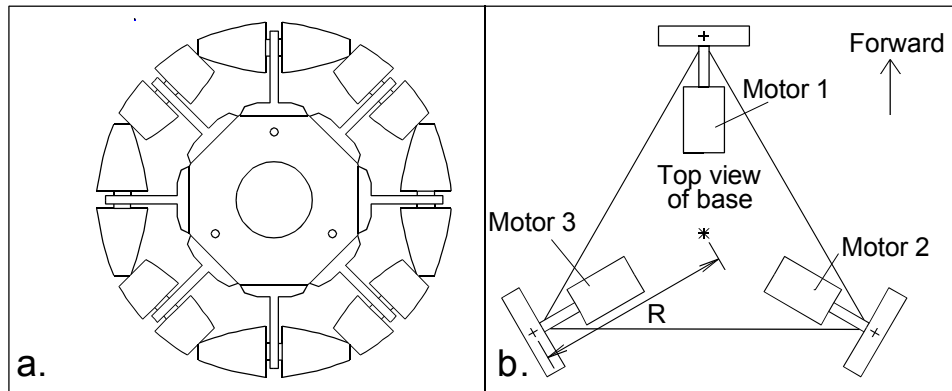


Figure 1.12: a. Schematic of the wheel assembly used by the Veterans Administration [La et al., 1981] on an omnidirectional wheelchair. b. Top view of base showing relative orientation of components in the three-wheel configuration. (Adapted from [Holland, 1983].)

$$\begin{aligned}
 V_1 &= \omega_1 r = V_x + \omega_p R \\
 V_2 &= \omega_2 r = -0.5V_x + 0.867V_y + \omega_p R \\
 V_3 &= \omega_3 r = -0.5V_x - 0.867V_y + \omega_p R
 \end{aligned}
 \tag{1.13}$$

where

$V_i$  = tangential velocity of wheel number  $i$   
 $\omega_i$  = rotational speed of motor number  $i$   
 $\omega_p$  = rate of base rotation about pivot axis  
 $\omega_r$  = effective wheel radius  
 $\omega_R$  = effective wheel offset from pivot axis.

### 1.3.6 Multi-Degree-of-Freedom Vehicles

Multi-degree-of-freedom (MDOF) vehicles have multiple drive and steer motors. Different designs are possible. For example, HERMIES-III, a sophisticated platform designed and built at the Oak Ridge National Laboratory [Pin et al., 1989; Reister et al., 1991; Reister, 1991] has two powered wheels that are also individually steered (see Figure 1.13). With four independent motors, HERMIES-III is a 4-degree-of-freedom vehicle.

MDOF configurations display exceptional maneuverability in tight quarters in comparison to conventional 2-DOF mobility systems, but have been found to be difficult to control due to their overconstrained nature [Reister et al., 1991; Killough and Pin, 1992; Pin and Killough, 1994; Borenstein, 1995]. Resulting problems include increased wheel slippage and thus reduced odometry accuracy. Recently, Reister and Unseren [1992; 1993] introduced a new control algorithm based on Force Control. The researchers reported on a substantial reduction in wheel

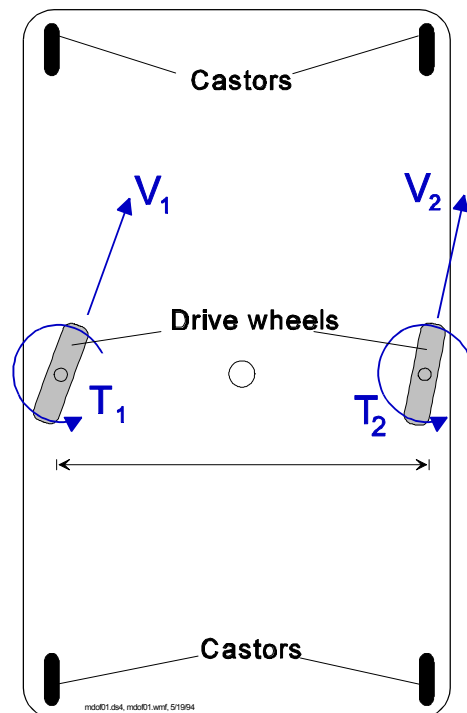


Figure 1.13: A 4-degree-of-freedom vehicle platform can travel in all directions, including sideways and diagonally. The difficulty lies in coordinating all four motors so as to avoid slippage.

slippage for their two-wheel drive/two-wheel steer platform, resulting in a reported 20-fold improvement of accuracy. However, the experiments on which these results were based avoided *simultaneous* steering and driving of the two steerable drive wheels. In this way, the critical problem of coordinating the control of all four motors *simultaneously and during transients* was completely avoided.

Unique Mobility, Inc. built an 8-DOF vehicle for the U.S. Navy under an SBIR grant (see Figure 1.14). In personal correspondence, engineers from that company mentioned to us difficulties in controlling and coordinating all eight motors.



**Figure 1.14:** An 8-DOF platform with four wheels individually driven and steered. This platform was designed and built by *Unique Mobility, Inc.* (Courtesy of [UNIQUE].)

### 1.3.7 MDOF Vehicle with Compliant Linkage

To overcome the problems of control and the resulting excessive wheel slippage described above, researchers at the University of Michigan designed the unique *Multi-Degree-of-Freedom* (MDOF) vehicle shown in Figures 1.15 and 1.16 [Borenstein, 1992; 1993; 1994c; 1995]. This vehicle comprises two differential-drive *LabMate* robots from [TRC]. The two *LabMates*, here referred to as “trucks,” are connected by a *compliant linkage* and two rotary joints, for a total of three internal degrees of freedom.

The purpose of the compliant linkage is to accommodate momentary controller errors without transferring any mutual force reactions between the trucks, thereby eliminating the excessive wheel slippage reported for other MDOF vehicles. Because it eliminates excessive wheel slippage, the MDOF vehicle with compliant linkage is one to two orders of magnitude more accurate than other MDOF vehicles, and as accurate as conventional, 2-DOF vehicles.

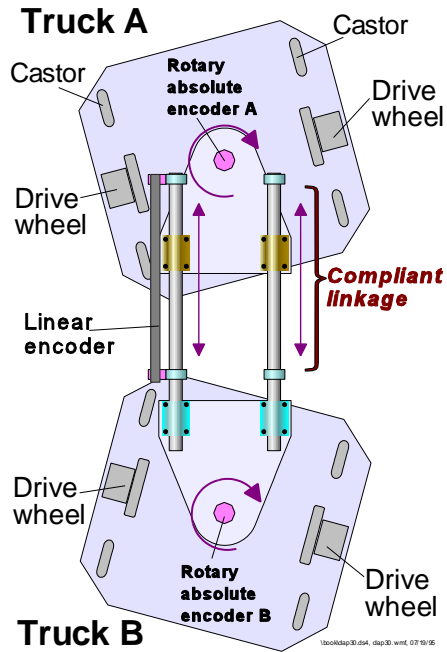


**Figure 1.15:** The compliant linkage is instrumented with two absolute rotary encoders and a linear encoder to measure the relative orientations and separation distance between the two trucks.



**Figure 1.16:** The University of Michigan's MDOF vehicle is a dual-differential-drive multi-degree-of-freedom platform comprising two TRC *LabMates*. These two "trucks" are coupled together with a *compliant linkage*, designed to accommodate momentary controller errors that would cause excessive wheel slippage in other MDOF vehicles. (Courtesy of The University of Michigan.)

### 1.3.8 Tracked Vehicles

Yet another drive configuration for mobile robots uses tracks instead of wheels. This very special implementation of a differential drive is known as *skid steering* and is routinely implemented in track form on bulldozers and armored vehicles. Such skid-steer configurations intentionally rely on track or wheel slippage for normal operation (Figure 1.17), and as a consequence provide rather poor dead-reckoning information. For this reason, skid steering is generally employed only in tele-operated as opposed to autonomous robotic applications, where the ability to surmount significant floor discontinuities is more desirable than accurate odometry information. An example is seen in the track drives popular with remote-controlled robots intended for explosive ordnance disposal. Figure 1.18 shows the Remotec *Andros V* platform being converted to fully autonomous operation (see Sec. 5.3.1.2).

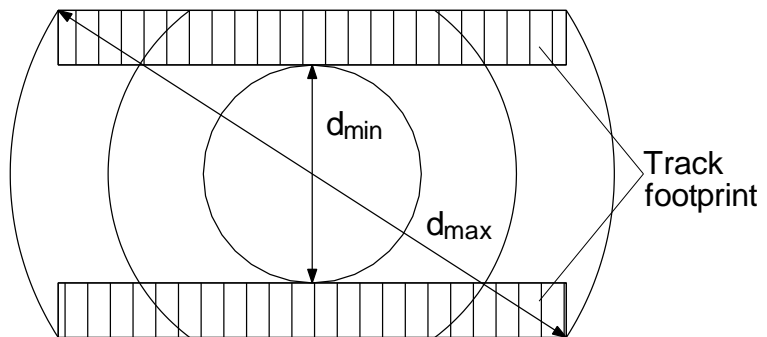


**Figure 1.17:** The effective point of contact for a skid-steer vehicle is roughly constrained on either side by a rectangular zone of ambiguity corresponding to the track footprint. As is implied by the concentric circles, considerable slippage must occur in order for the vehicle to turn [Everett, 1995].

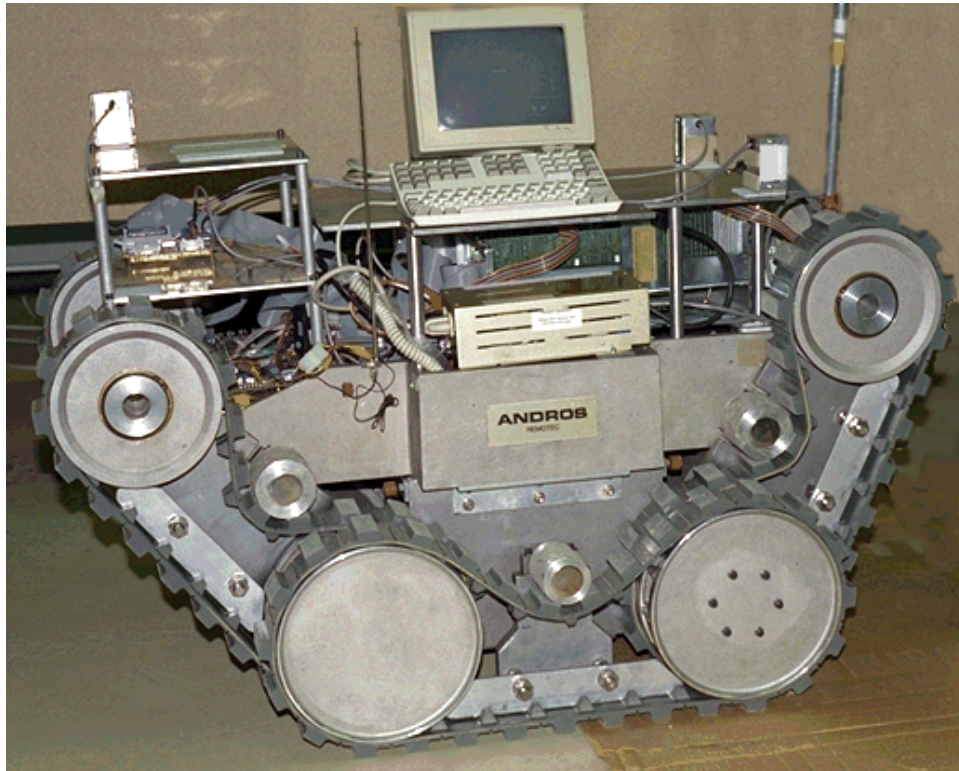


**Figure 1.18:** A Remotec *Andros V* tracked vehicle is outfitted with computer control at the University of Michigan. Tracked mobile platforms are commonly used in tele-operated applications. However, because of the lack of odometry feedback they are rarely (if at all) used in fully autonomous applications. (Courtesy of The University of Michigan.)